The Response of Gfrp Nanocomposites Reinforced with Functionalized SWCNT under Low Velocity Impact: Experimental and Ls-Dyna Simulation Investigations

Mohammad Ali Maghsoudlou[1]*, Reza Barbaz Isfahani[1], Saeed Saber-Samandari[2], Mojtaba Sadighi[1]

* maghsoudlou.ma@gmail.com
[1] Department of Mechanical Engineering, Amirkabir University of Technology, Tehran, Iran
[2] New Technologies Research Center, Amirkabir University of Technology, Tehran, Iran

Abstract: The low velocity impact (LVI) response of a pure and glass fiber reinforced polymer composites (GFRP) with 0.1, 0.3 and 0.5 wt.% of functionalized single-walled carbon nanotubes (SWCNTs) was experimentally investigated. LS-DYNA simulation was used to model the impact test of pure and incorporated GFRP with 0.3 wt. % of SWCNT in order to compare experimental and numerical results of LVI tests. All tests were performed at two different levels of energy. At 30J energy, the specimen containing 0.5 wt. % SWCNT was completely destructed. The results showed that the incorporated GFRP with 0.3 wt. % SWCNT had the highest energy absorption and the back-face damage area of this sample was smaller than other specimens. TEM images from specimens were also analyzed and showed the incorporation of well-dispersed 0.1 and 0.3 wt. % of SWCNT, while in specimens containing 0.5 wt.% of CNT, tubes tended to be agglomerated causing a drop in the LVI response of the specimen. The contact time of the impactor in numerical and experimental results was approximately equal. However, as the conditions in numerical modeling are considered ideal, the maximum contact forces in LS DYNA simulation results were higher than the experimental results.

Keywords: Energy absorption, Functionalized single-walled carbon nanotube, Low velocity impact, LS-DYNA simulation, Polymer composites

1. INTRODUCTION

The use of fiber reinforced polymer composites (FRPs) is enhancing in different engineering applications, such as airplane components, marine structures, and civil because of their high specific strength and stiffness [1- 3]. In recent decades, some researchers have studied the addition of nanoparticles such as carbon nanotubes (CNTs) to improve the FRP properties [4- 7]. Also, the addition of single walled carbon nanotubes (CNTs) with unique physical properties like high strength and aspect ratio attracted researchers. This is because the resulting composites were synchronously reinforced and functionalized with both of micron diameter fibers and nano-scale fillers [8- 11]. On the other hand, these resulting composites can be exposed to LVI loadings during operation [12].

Many researchers reported the importance of LVI behavior of FRPs and investigated LVI properties analytically, experimentally and numerically [13- 17]. Among those investigations, Soto et al. [18] developed an efficient numerical model to better understand the damage mechanisms and their sequence during the LVI. Their numerical models showed that matrix cracking can be negligible while delamination and especially the fiber constitutive law shape are important parameters. Patel et al. [19] performed the stochastic dynamic response of FRP plate subjected to LVI considering the damage evaluation based on failure criteria and developed a stochastic progressive damage model. They claimed that in their case study, there was a possibility of underestimation of the peak contact force and displacement by 28% and 22% respectively if the scatter in the material properties and impactor velocity were not considered.

Also, the incorporation of CNT into FRPs can enhance the impact response and restrict the damage size in the resulted composites [20-22]. Jam et al. [23] analyzed the response of functionally graded CNT reinforced composite beams under LVI based on the first order Timoshenko beam theory. They showed that total volume fraction of CNT was an important factor in LVI response and their numerical results indicated that, increasing the volume fraction of CNT increased the contact force, whereas decreases the contact time and the maximum indentation. Kostopoulos et al. [24] investigated

Mohammad Ali Maghsoudlou, Reza Barbaz Isfahani, Saeed Saber Samandari, Mojtaba Sadighi

the effect of multi-wall carbon nanotubes (MWCNTs) on the impact behavior of carbon fiber reinforced polymer (CFRP) laminates. They manufactured CFRP laminates using epoxy matrix (Bisphenol A) incorporated with 0.5 wt% MWCNT. The resulted composites were subjected to LVI test and their results showed no specific difference for the delamination area or the absorbed energy per unit delamination area in comparison with neat specimens. Ashrafi et al. [25] used CNT to develop nano-modified carbon fiber/epoxy laminates. They performed impact and compression-after-impact tests on laminates with and without CNT and found that incorporation of only 0.1 wt% of CNT resulted in a 5% reduction of the area of impact damage and a 3.5% increase in compression-after-impact strength. Soliman et al. [26] studied the LVI response of thin carbon woven fabric composites reinforced with functionalized MWCNT. They fabricated three types of multi-scale composites containing 0.5, 1.0, and 1.5 wt% of MWCNT and performed high velocity impact at different levels of energy. They showed that incorporation of MWCNT enhanced the impact response and limited the damage size in the woven carbon fiber composite. For example, they indicated, the addition of 1.5% MWCNTs resulted in 50% increase in energy absorption. Taraghi et al. [27] examined the LVI response of woven Kevlar/epoxy laminated composites enhanced with 0.3, 0.5 and 1 wt% of MWCNT. They claimed that the incorporation of MWCNTs improved the impact response and restricted the damage size in the woven Kevlar fiber composites at ambient and low temperature. Tehrani et al. [28] investigated the impact resistance and impact damage progression of CFRP enhanced by the addition of MWCNT. Their results indicated that incorporating of 2 wt% of MWCNT into the CFRP increased the absorbed impact energy by 21%. Also, they discussed the consequences of adding MWCNT to the matrix of CFRP on the impact progressive damage and energy in terms of the damage mechanisms. Singh et al. [29] investigated LVI response of glass/MWCNT/epoxy composites. Their results showed that the energy absorption was improved by 14.91% and 48.26% (at 4.5 and 5.5 m/s, respectively) by addition of 0.3 wt% of MWCNT and the damage area was minimum at 3 wt% of MWCNT.

Also, the use of analytical and numerical methods could be helpful in having a better perception of physical parameters of LVI tests [30- 33]. Ghasemnejad et al. [34] investigated the impact damage response of artificial single and multi-delaminated FRP composites and also simulated the Charpy impact test of delaminated composite beams by finite element (FE) software LS-DYNA to verify FE results with the relevant experimental results. They claimed that the FEA simulation was in good agreement with the results obtained for the Charpy impact test of multi-delaminated composite beams. Heimbs et al. [35] developed finite element models for impact simulations of a sandwich structures with textile-reinforced composite with LS-DYNA. They showed that their simulation results correlated well with test data which allowed them for efficient parameter studies or detailed evaluations of damage patterns and energy absorption mechanisms. Hosseinzadeh et al. [15] fabricated four different fiber reinforced composite plates and studied their damage behavior. They also modeled all the plates using ANSYS LS-DYNA V6.1 under similar conditions to the experiments. They observed that the damage zone shapes derived from software modeling did not show a good coincidence with experimental results. Hufenbach et al. [36] investigated the LVI response of carbon reinforced composites experimentally and numerically by using an orthotropic continuous damage-based material approach available in LS-DYNA. They observed a good correlation between experimental and numerical results including forces and failure modes. Sevkat et al. [37] used LS-DYNA with the Chang–Chang linear-orthotropic damage model to compare FEA and experimental results of ballistic impact response of S2-glass fiber/toughened epoxy composite beams. They found a good agreement between experimental and FE results. They observed delamination, matrix failure, fiber breakage and projectile deformation during the impact tests and claimed that nonlinear-orthotropic material model predicted these failure modes with a good accuracy.

As the above literature survey indicates and regarding to the previous studies on the LVI tests on glass fiber reinforced polymer composites (GFRP), there is no specific study on the effect of functionalized COOH-SWCNT on the impact

2

response of enhanced GFRP by different loading of SWCNT. As a result, the LVI response of incorporated GFRP with functionalized SWCNT needs further investigation. Therefore, in the present study the effect of the incorporation of the functionalized SWCNT with different loadings on the LVI response of GFRP was investigated. Also, the impact process of neat and incorporated GFRP with 0.3 wt% of functionalized SWCNT was simulated by FE software LS-DYNA and the results were compared with experimental results. Finally, the enhancement mechanisms of SWCNT on the LVI response of GFRP with different loadings were discussed.

2. EXPERIMENTAL PROCEDURES

Bisphenol-F type epoxy resin and hardener supplied from Chang Chun Plastics Co., China were selected to use as the matrix of GFRP. The functionalized COOH-SWCNT (purity>95% and outer diameter: 1-2 nm) was purchased from US Research Nanomaterials, Inc., USA. Uni-Directional (UD) glass fiber, 400 g/m^2, was obtained from Mytex Turkey to use as the main reinforcement of GFRP.

One of the most significant challenges during the manufacture of the incorporated FRPs with

One of the most significant challenges during the manufacture of the incorporated FRPs with SWCNT is to benefit the enhanced properties of resin in the composites [4]. High power dispersion sonicating method and high-speed shearing were selected as described in [8, 38] to disperse the SWCNT into epoxy resin. Neat GFRP and enhanced GFRP containing 0.1, 0.3 and 0.5 wt% of COOH-SWCNT were fabricated as shown in Figure 1.

First, the desired amounts of COOH-SWCNT contents were weighed carefully and mixed with the required amount of Bisphenol-F type epoxy resin and stirred for 15 min at 1500 rpm. Then, the mixtures containing 0.1, 0.3 and 0.5 wt% of COOH-SWCNT were sonicated in ice-bath (to keep the temperature around 50˚C) for 30 min, 40 min and 60 min, respectively.

After providing the reinforced resin, the desired amount of hardener was mixed at a mass ratio of 100/10. After mixing the resin and the hardener, the mixture was degassed for 20 min in a vacuum oven. Then, all the laminated composite specimens (pure and multi-scale composites) were fabricated with Hand Lay-up process by using six ply laminates with stacking sequence [0/90/0]s. Finally, vacuum pressure was applied for 48h at 25°C.
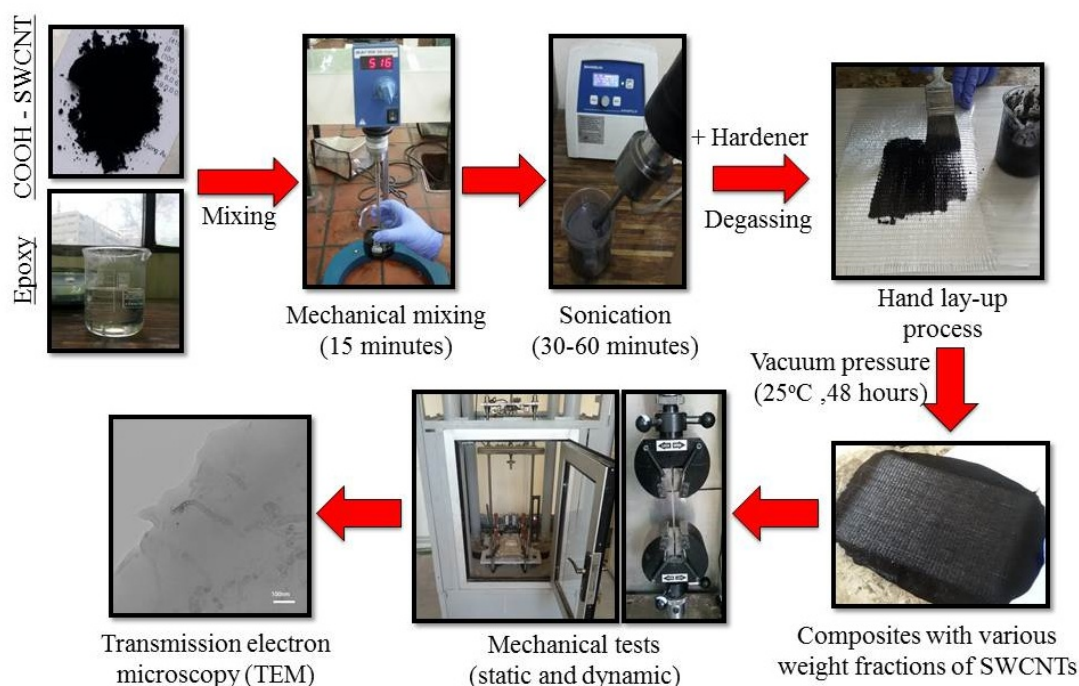

Fig. 1. A schematic of fabrication process for incorporated GFRP plates with COOH-SWCNT using for LVI and mechanical properties tests

3

Mohammad Ali Maghsoudlou, Reza Barbaz Isfahani, Saeed Saber Samandari, Mojtaba Sadighi

1.1. Specimen configurations and test procedures

LVI tests were performed using the drop-weight impact machine as illustrated in Figure2. The mass and height of the impactor can be changed to provide the desired velocities and impact energies. The diameter and the weight of the impactor were 15 mm and 3.27 Kg, respectively. As Figure 2 shows, additional weights can be added to the carriage, at the top of the set up to increase the subjected energy. The GFRP plates were subjected to two levels of energy including 21J and 30J. The LVI test specimens were cut from the GFRP plates with the dimensions of 120 mm ×120 mm. The impact was carried out on the center of the fabricated plates whose edges were fully clamped at each side. To measure the force-time history of the plate during the impact, the impactor was equipped with an accelerometer connected to software to calculate the data. Also, the absorbed energy can be calculated by force-displacement diagrams obtained from the LVI tests.
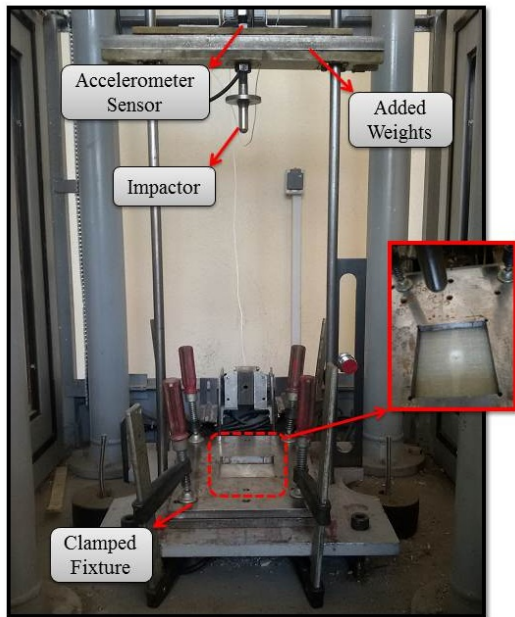

Fig. 2. The LVI test setup.

The mechanical properties of neat and incorporated 0.3 wt% of COOH-CNT glass/epoxy were obtained experimentally according to the ASTM D3518 for in-plane shear response (S_c and G_{12}), ASTM D3039 for longitudinal and transverse tensile strength and modulus (X_t, Y_t, E_{11} and E_{22}) and ASTM D3410 for longitudinal and transverse compressive strength

(X_c and Y_c) standards to perform numerical simulation using FE software LS-DYNA.

The damage area of the incorporated GFRP specimens were comparatively examined using transmission electron microscopy (TEM) (Zeiss EM10C) after the LVI tests, in order to inspect the state of CNTs dispersion and enhancement mechanisms of the SWCNTs.

In this study, LS-DYNA numerical explicit finite element code was used to simulate the impact process of neat and incorporated GFRP with 0.3 wt% of functionalized SWCNT. This code has many different composite failure models, where MAT54 code material card was selected in this study. MAT54 uses Chang–Chang failure criterion which is only valid for thin shell elements [39, 40]. According to this failure criterion, tensile failure in fiber direction and matrix direction respectively are defined by equation (1) and (2), and compressive failure in fiber direction and matrix direction respectively are defined by equation (3) and (4).

$$\sigma_{aa} \succ 0 \Rightarrow e_f^2 = \left(\frac{\sigma_{aa}}{X_t}\right)^2 + \left(\frac{\sigma_{ab}}{S_c}\right)^2 - 1 \begin{cases} e_f \geq 0 & failed \\ e_f < 0 & elastic \end{cases} \tag{1}$$

$$\sigma_{bb} \succ 0 \Rightarrow e_m^2 = \left(\frac{\sigma_{bb}}{Y_t}\right)^2 + \left(\frac{\sigma_{ab}}{S_c}\right)^2 - 1 \begin{cases} e_m \geq 0 & failed \\ e_m < 0 & elastic \end{cases} \tag{2}$$

$$\sigma_{aa} \prec 0 \Rightarrow e_f^2 = \left(\frac{\sigma_{aa}}{X_c}\right)^2 - 1 \begin{cases} e_f \geq 0 & failed \\ e_f < 0 & elastic \end{cases} \tag{3}$$

$$\sigma_{bb} \prec 0 \Rightarrow e_m^2 = \left(\frac{\sigma_{bb}}{2S_c}\right)^2 + \left[\left(\frac{Y_c}{2S_c}\right)^2 - 1\right]\frac{\sigma_{bb}}{Y_c} + \left(\frac{\sigma_{ab}}{S_c}\right)^2 - 1 \begin{cases} e_m \geq 0 & failed \\ e_m < 0 & elastic \end{cases} \tag{4}$$

Where σ_{aa} is stress in the fiber direction, σ_{bb} is stress in matrix direction, σ_{ab} is in-plane shear stress, X_t is longitudinal tensile strength, X_c is longitudinal compressive strength, Y_t is transverse tensile strength, Y_c is transverse compressive strength and S_c is in-plane shear strength. Also, MAT 54 material models consist of failure strains such as tensile failure strain in fiber direction as DFAILT parameter and compressive failure strain as DFAILC parameter which are defined by linear functions shown as follows:

$$DFAILT = \frac{X_t}{E_1} \tag{5}$$

$$DFAILC = \frac{X_c}{E_1} \tag{6}$$

These parameters obtained experimentally and reported in the experimental results section.

As shown in Figure 3, six-ply laminates with stacking sequence [0/90/0]S and 2.4 mm in

4

thickness were modeled as the shell layer and were meshed by shell element. The clamped boundary conditions were considered for composite laminates and all degrees of freedom for the impactor were closed, except the transitional mode in the Z direction. The velocity at which the impactor strikes was attributed by Initial-Velocity in view of the impact energy. Impactor and laminate layers were modeled as the master surface and slave surface, respectively. Additionally, according to Berk et al. [12], the static and dynamic friction coefficients were chosen to 0.3 and 0.1, respectively. Contact-Automatic-Surface-To-Surface-Tiebreak was used to avoid merging layers into each other during the impact.
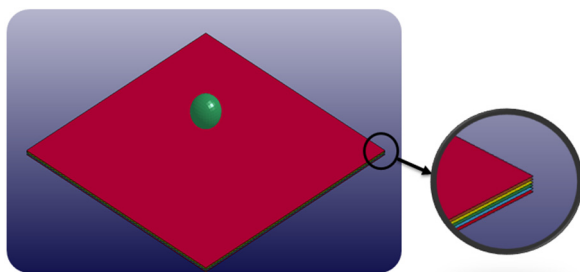

Fig. 3. View of shell layers and impactor in LS-PrePost

The steel-made impactor was modeled by MAT_RIGID 20 with the elastic modulus of 200 GPa, the density of 7860 Kg/m^3 and Poisson ratio of 0.3. In view of the convergence analysis of responses, the composite laminates and impactor elements were considered in square form with the side length of 2 mm.

3. RESULTS AND DISCUSSION

In this study, LVI response of pure and incorporated GFRP with 0.1, 0.3 and 0.5 wt% of functionalized SWCNT subjected to the 21 and 30J energy was investigated. Figure 4 shows the force-time histories of all specimens.
As it is seen from Figure 4, in each energy level, no significant difference is observed on the maximum contact force among the specimens. This can be due to the fact that between two reinforcements of SWCNT and fibers, the fiber tolerates the imposed force and the role of SWCNT is a little for tolerating the maximum force.
The contact time duration in all specimens is approximately equal in both energy levels. This

trend is not observed for specimen containing 0.5 wt% of SWCNT subjected to 30J energy and the diagram has great mutations after the maximum force and its contact time duration cannot be computed from the diagram. Due to the destruction of this specimen after the impact, it was not possible to properly measure the contact data for this sample.
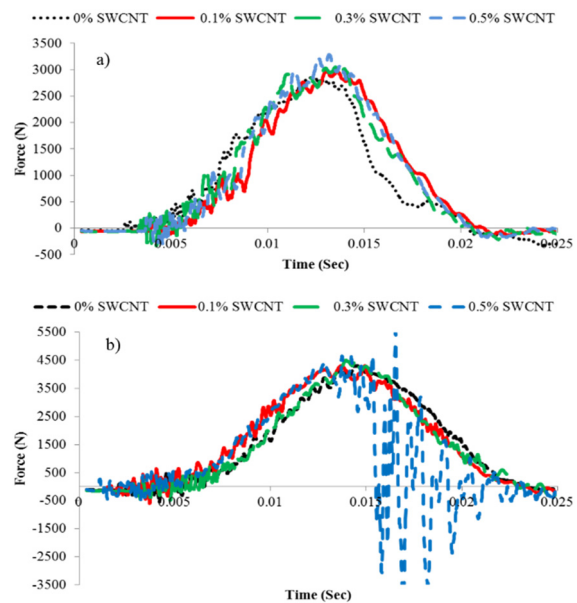

Fig. 4. Load history of GFRP specimens a) under the 21J energy and b) the 30J energy for various contents of SWCNT.

Comparing the load history in the both levels of energy and back-face damage of specimens, any significant fluctuations and mutations on the force-time diagram can construe a kind of destruction in the composite material. In fact, the small mutations can be attributed to the matrix crack and the large mutations and fluctuations can be considered as the fibers rupture. It should also be noted that the local and miniscule fluctuations in the whole time interval of diagrams are related to the vibrations between the sheet and impactor and should not be considered as the failure.
The displacement-force diagrams during the impact test are shown in Figure 5. In view of the time-force diagram for the specimen containing 0.5 wt% of SWCNT and its failure in 30J energy level, the displacement-force diagram cannot be plotted for this sample and the amount of energy absorption cannot be defined for it. By calculating the area under the displacement-force diagram, the amount of absorbed energy for each specimen is shown in Table 1.
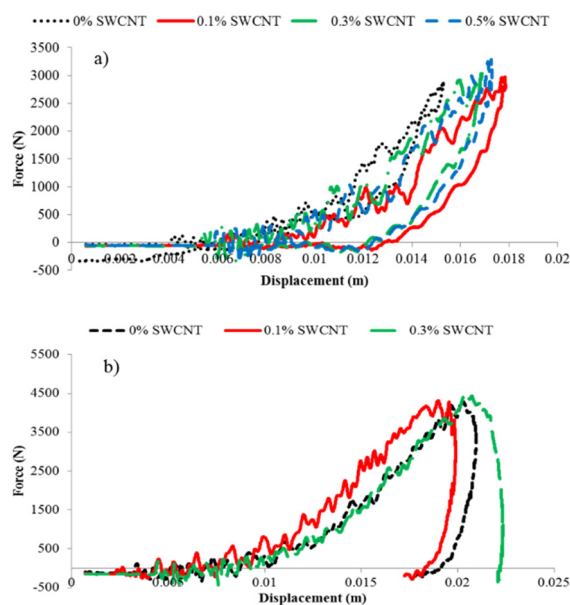
Mohammad Ali Maghsoudlou, Reza Barbaz Isfahani, Saeed Saber Samandari, Mojtaba Sadighi

Fig. 5. Force–displacement curves for a) 21J energy and b) 30J energy

With regards to the displacement-force diagram in 21 J energy level, the forth and back paths of the impactor match with each other for the pure specimen. It means that this specimen has approximately behaved elastically during the contact and due to this issue; its energy absorption amount is lower than other specimens. But in specimens containing 0.1, 0.3 and 0.5 wt% of SWCNT, the forth and back paths do not match indicating the specimens showed more brittle behavior because of adding the SWCNT.

As the energy level increases to 30 J, it is observed that specimens, especially specimen containing 0.3 wt% of SWCNT, have considerable permanent changes in forth and back

path of the impactor and they are on the threshold of failure.

As the results of energy absorption indicated, once the weight percent increased to 0.3 %, the energy was absorbed more and as it increased to 0.5 %, the absorption decreased in 21J energy level and the specimen failed in 30J. This can be due to the SWCNT agglomeration and its non-uniform distribution in the matrix and as a consequence, weakening of matrix by an increase in the weight percent of SWCNT. To investigate this issue, TEM pictures of specimens were analyzed, as shown in Figure 6.
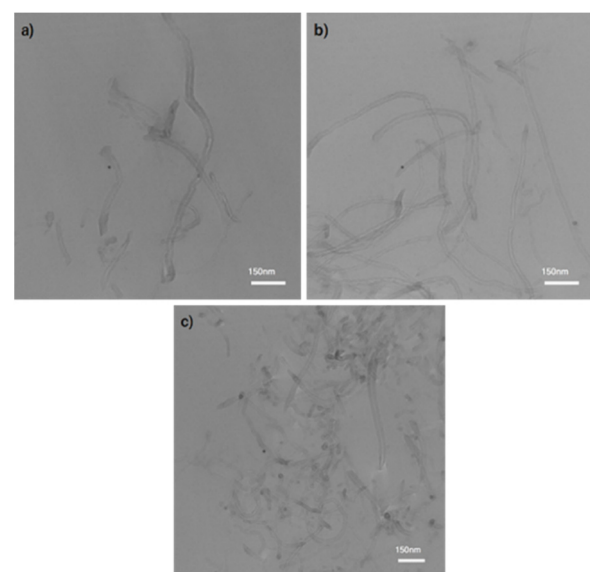

Fig. 6. TEM images: the state of dispersion of SWCNT in incorporated GFRP with a) 0.1 wt%, b) 0.3 wt% and c) 0.5 wt% of SWCNT.

Figures 6(a) and 6(b) show the incorporation of a

Table 1. The absorbed energy and the percent of absorption of incorporated GFRP with different weight percent of SWCNT

| Weight percent of SWCNT | Impact energy | | | |
| | 21J | | 30J | |
	Absorbed energy (J)	Percent of absorption	Absorbed energy (J)	Percent of absorption
0%	4.84	23.05	21.70	72.33
0.1%	7.40	35.24	24.26	80.87
0.3%	8.16	38.86	27.25	90.83
0.5%	7.93	37.76	-	-

well-dispersed 0.1 and 0.3 wt% of SWCNT, while as shown in Figure 6(C), in specimens containing 0.5 wt% of SWCNT, nanotubes tended to be agglomerated which caused a drop in mechanical properties because of stress concentration. This trend of decreasing the mechanical properties of composites along by the increasing the weight percent of SWCNT was reported in previous studies as well [5, 8, 41].

Comparing the back-face damage area in Figure 7, it can be concluded that energy absorption in the specimen appears as fibers rupture and matrix cracking. The increasing impact energy has led to larger back-face damage area such that on the specimen containing 0.5 wt% of SWCNT, it was completely destructed in 30J energy.
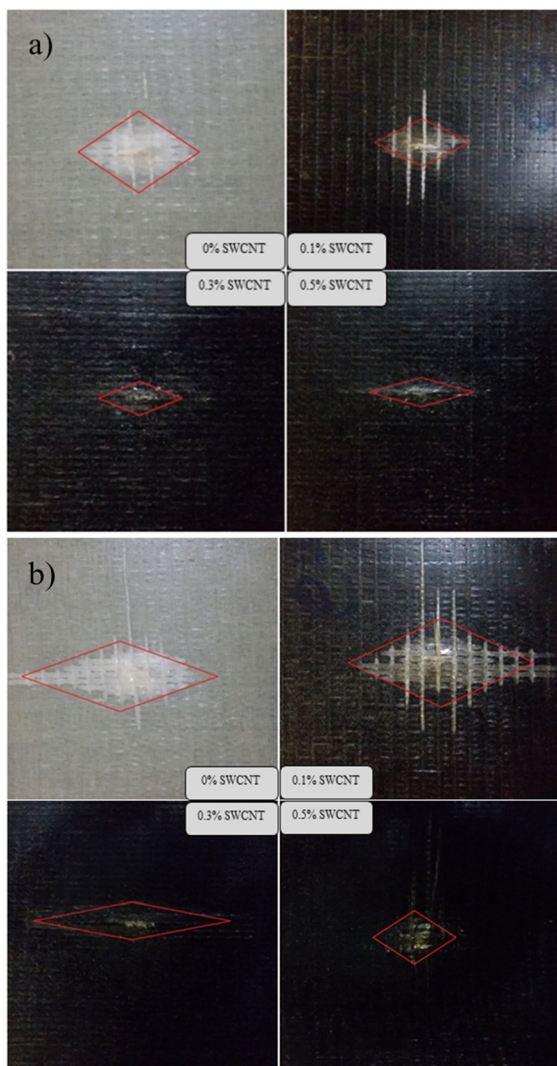
As shown in Figure 8, the main effect of incorporating SWCNT is the reinforcement of epoxy matrix and decreased the growth of matrix crack and reduced area off failure. On the other hand, SWCNT resistance to the cracking penetration and consequently decreasing failure area has raised the failure intensity on the small region under the impactor where such focus of failure is not desired.
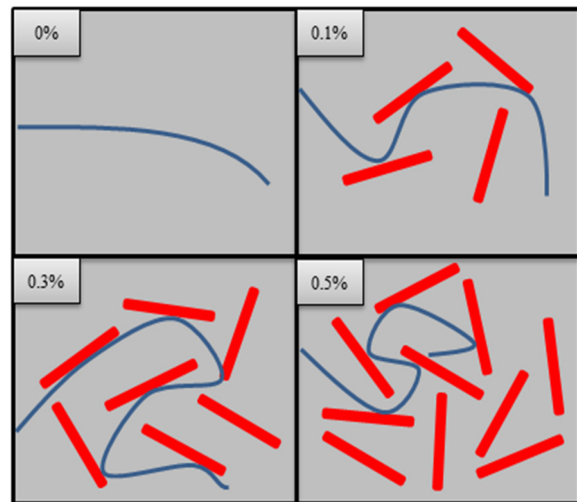

Fig. 8. A schematic of crack arresting (the blue lines show the crack growth and the red cylinders show the SWCNTs).

As mentioned earlier, the mechanical properties of the neat and incorporated GFRP with 0.3 wt% of SWCNT were obtained according to ASTM standards and summarized in Table 2 to simulate LVI tests using LS-DYNA software.

The force-time diagrams obtained from the LS-DYNA simulation are compared with experimental diagrams in Figure 9. As can be observed from the diagrams, the general trends of two numerical and experimental diagrams are the same for two pure and incorporated GFRP with 0.3 wt% of SWCNT specimens.

At the end of impactor contact, there is a small mutation on the numerical diagram for both specimens in both energy levels, which such phenomenon can be due to the reversal of stress wave from the support and reaching to the impactor location, while in the experimental results, these mutations are trivially seen. Meanwhile, the contact time of impactor in numerical and experimental results is approximately equal for two energy levels and matches well. If the maximum force between the numerical and experimental diagrams is considered as the criterion, the difference percentage of these results can be seen within the ones shown in Table 3.

Fig. 7. Comparative images of back-face damage for different incorporated GFRP with SWCNT subjected to a) 21J energy and b) 30J energy.

Mohammad Ali Maghsoudlou, Reza Barbaz Isfahani, Saeed Saber Samandari, Mojtaba Sadighi

Table 2. Mechanical properties of neat and enhanced GFRP for MAT54 code material.

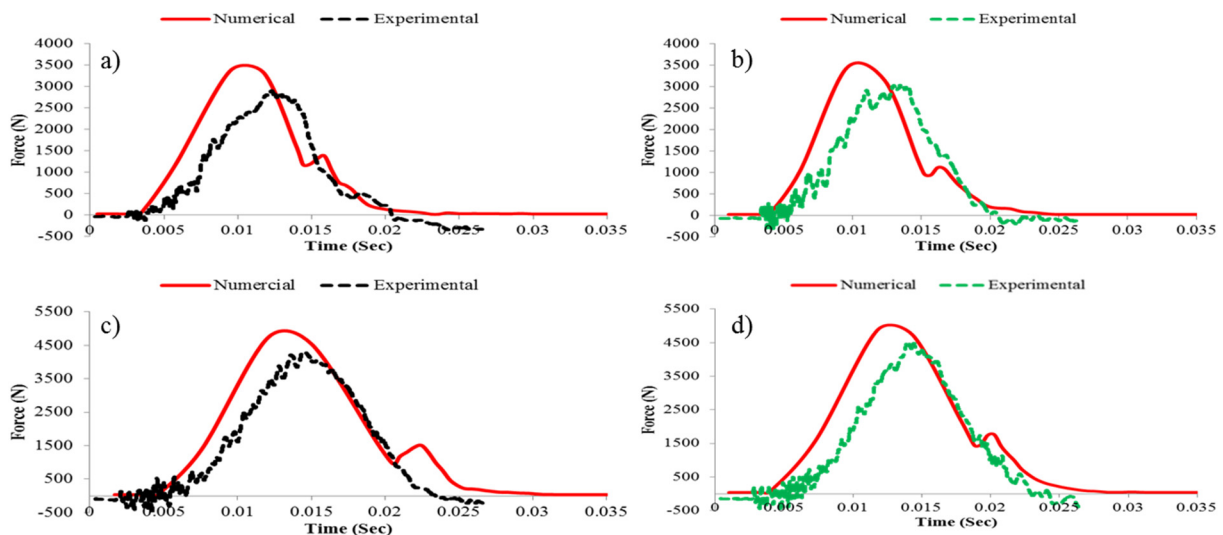| Properties	Neat GFRP (MPa)	Standard Deviation	0.3 wt% CNT + GFRP	Standard Deviation
E_{11}	32510.78	± 390.13	39143.28	± 874.68
E_{22}	8791.37	± 131.58	10330.61	± 242.31
G_{12}	3483.73	± 64.91	4032.07	± 94.51
S_c	78.54	± 1.76	89.94	± 2.85
X_t	478.32	± 5.35	523.03	± 15.36
Y_t	57.44	± 0.82	76.28	± 1.63
X_c	168.22	± 2.29	178.71	± 4.92
Y_c	48.93	± 0.75	54.49	± 1.05
DFAILT	0.0147	-	0.0134	-
DFAILC	0.0052	-	0.0046	-

Fig. 9. Comparative force- time response obtained from experimental and numerical investigation for: a and c) pure GFRP subjected to 21 and 30J energy, b and d) incorporated GFRP with 0.3 wt% of SWCNT subjected to 21 and 30J energy.

Table 3. Comparison between the maximum contact force of experimental and numerical LVI test results

Weight percent of SWCNT	Maximum contact force					
	21J			30J		
	Experimental	Numerical	Error %	Experimental	Numerical	Error %
0%	2880	3490	17.5	4330	4930	12.2
0.3%	3070	3560	13.8	4520	5040	10.3

As seen in Table 3, the presented values in numerical results are higher than the experimental ones. The reason can be stated that the drop in properties during the low velocity impact test is practically possible, where such issue is not seen in the numerical simulation. In other words, in the numerical model, properties are considered ideal, while this is no so in experimental conditions.

In Figure 10, LS-DYNA simulation images of back-face damage are observed which is consistent with the back-face damage in experimental ones in accordance with Figure 7.

Like the back-face damage in experimental results, once the weight percent of SWCNT increases, the back-face damage reduces and is focused on a smaller area under the impactor.

Fig. 10. Comparative LS DYNA simulation images of back-face damage for pure and incorporated GFRP with 0.3 wt% of SWCNT subjected to 21 and 30J energy.

4. CONCLUSIONS

In this study, low velocity impact response of reinforced GFRP with different loadings of (0.1, 0.3 and 0.5 wt. %) functionalized SWCNT was experimentally investigated. Also, to compare experimental and numerical results, LS-DYNA was utilized to simulate the LVI test on pure and specimen containing 0.3 wt. % of SWCNT. All specimens were tested under two impact energies including 21 and 30 J. In addition, TEM and the back-face damage images were studied and the reinforcement mechanisms were discussed. Based on the results obtained from the experiments and numerical simulation, the following conclusions are reached:

1. Fibers played more pivotal role to tolerate the applied impact force compared to SWCNTs in GFRP composite plates.
2. Any fluctuations on the force-time diagram can be considered as a type of destruction in the specimen which can be determined according to the size of fluctuation.
3. The agglomeration of SWCNTs resulted in a drop in LVI response of specimen with 0.5 wt. % of SWCNTs.
4. The increase in impact energy led to a larger back-face damage area while the specimen containing 0.5 wt. % of SWCNT was completely destructed under 30J energy.
5. The images of back-face damage showed that SWCNT resistance to crack penetration and decreasing failure area has raised the failure intensity on the small region under the impactor.
6. A small mutation at the end of the numerical force-time diagram was observed. This phenomenon can be related to the reversal of stress wave from the support and reaching to the impactor location.
7. A drop in properties during the LVI tests led to the higher maximum forces in numerical results in comparison with experimental data.

5. REFERENCES

[1] Rahmandoust, M. and Ayatollahi, M.R., Characterization of carbon nanotube based composites under consideration of defects. Switzerland, Springer International Publishing, switzerland, 2016, 112-185.

[2] Kamarian, S, Bodaghi, M, Barbaz Isfahani, R. and Song, J-i, "A comparison between the effects of shape memory alloys and carbon nanotubes on the thermal buckling of laminated composite beams." Mechanics Based Design of Structures and Machines, 2020, 1-24.

[3] Roustazadeh, D, Aghadavoudi, F. and Khandan, A, "A synergic effect of CNT/Al₂O₃ reinforcements on multiscale epoxy-based glass fiber composite: fabrication and molecular dynamics modeling." Molecular Simulation, 2020, 46(16), 1308-19.

[4] Moghimi monfared, R, Ayatollahi, M.R. and Barbaz Isfahani, R., "Synergistic effects of hybrid MWCNT/nanosilica on the tensile and tribological properties of woven carbon fabric epoxy composites." Theoretical and Applied Fracture Mechanics, 2018, 96, 272-84.

[5] Barbaz-I, R., Experimental determining of the elastic modulus and strength of composites reinforced with two nanoparticles, MSc Thesis, Department of Mechanical Engineering Iran University of Science and Technology, Tehran, 2014.

[6] Maghsoudlou, M.A., Barbaz Isfahani, R, Saber-Samandari, S. and Sadighi M, "Effect of interphase, curvature and agglomeration of SWCNTs on mechanical properties of polymer-based nanocomposites: experimental and numerical investigations." Composites Part B: Engineering. 2019. 175, 107-119.

[7] Mohammadimehr, M. and Alimirzaei, S, "Nonlinear static and vibration analysis of Euler-Bernoulli composite beam model reinforced by FG-SWCNT with initial geometrical imperfection using FEM." Structural Engineering and Mechanics, 2016, 59(3), 431-54.

[8] Ayatollahi, M.R., Barbaz Isfahani, R. and Moghimi monfared, R, "Effects of multi-walled carbon nanotube and nanosilica on tensile properties of woven carbon fabric-reinforced epoxy composites fabricated using VARIM." Journal of Composite Materials, 2017, 51(30), 4177-88.

[9] Maghsoudlou, M.A., Nassireslami, E, Saber-Samandari, S. and Khandan, A, "Bone regeneration using bio-nanocomposite tissue reinforced with bioactive nanoparticles for femoral defect applications in medicine." Avicenna Journal of Medical Biotechnology, 2020, 12(2), 68-76.

[10] Moeini, M, Barbaz Isfahani, R, Saber-Samandari S. and Aghdam, M,M., "Molecular dynamics simulations of the effect of temperature and strain rate on mechanical properties of graphene–epoxy nanocomposites." Molecular Simulation, 2020, 46(6), 476-86.

[11] Kamarian, S, Bodaghi, M, Barbaz Isfahani, R. and Song, J-i, "Thermal buckling analysis of sandwich plates with soft core and CNT-Reinforced composite face sheets." Journal of Sandwich Structures & Materials, 2020, 1099636220935557.

[12] Berk, B, Karakuzu, R, Murat Icten, B, Arikan, V, Arman, Y, Atas, C. and et al., "An experimental and numerical investigation on low velocity impact behavior of composite plates." Journal of Composite Materials, 2016, 50(25), 3551-3559.

[13] Heydari Meybodi, M, Saber-Samandari, S. and Sadighi, M., "An experimental study on low-velocity impact response of nanocomposite beams reinforced with nanoclay." Composites Science and Technology, 2016, 133, 70-8.

[14] Heydari Meybodi, M, Saber-Samandari, S. and Sadighi M., "Experimental dynamic analysis of polymer-based nanocomposite beams under low-velocity impact loading." Iranian Polymer Journal, 2017, 26(12), 929-40.

[15] Hosseinzadeh, R, Shokrieh, M.M. and Lessard, L., "Damage behavior of fiber reinforced composite plates subjected to drop weight impacts." Composites science and technology, 2006, 66(1), 61-8.

[16] Bagheri, S, Hashemian, M, Khosravi, M. and Khandan A., "An experimental investigation of novel hybrid epoxy / glass fibers nanocomposite reinforced with nanoclay with enhanced properties for low velocity impact test." Journal of Nanostructures, 2020, 10(1), 92-106.

[17] Hasanzadeh, R, Azdast, T, Eungkee Lee, R. and Afsari Ghazi, A., "Experimental polymeric nanocomposite material selection for automotive bumper beam using multi-criteria decision making methods." Iranian Journal of Materials Science and

Engineering, 2017, 14(3), 1-10.

[18] Soto, A, González, E, Maimí, P, de la Escalera, F.,M., de Aja, J.S. and Alvarez, E., "Low velocity impact and compression after impact simulation of thin ply laminates." Composites Part A: Applied Science and Manufacturing, 2018, 109, 413-27.

[19] Patel, S. and Soares, C.G., "Reliability Assessment of Glass Epoxy Composite Plates due to Low Velocity Impact." Composite Structures, 200, 2018, 659-668.

[20] Sharma, S. and Lakkad, S., "Impact behavior and fractographic study of carbon nanotubes grafted carbon fiber-reinforced epoxy matrix multi-scale hybrid composites." Composites Part A: Applied Science and Manufacturing, 2015, 69, 124-31.

[21] Siegfried, M, Tola, C, Claes, M, Lomov, S.V., Verpoest, I. and Gorbatikh, L., "Impact and residual after impact properties of carbon fiber/epoxy composites modified with carbon nanotubes." Composite Structures, 2014, 111, 488-96.

[22] Kamarian, S, Bodaghi, M, Barbaz Isfahani, R, Shakeri, M. and Yas, M., "Influence of carbon nanotubes on thermal expansion coefficient and thermal buckling of polymer composite plates: experimental and numerical investigations." Mechanics Based Design of Structures and Machines, 2019, 1-16.

[23] Jam, J. and Kiani, Y., "Low velocity impact response of functionally graded carbon nanotube reinforced composite beams in thermal environment." Composite Structures, 2015, 132, 35-43.

[24] Kostopoulos, V, Baltopoulos, A, Karapappas, P, Vavouliotis, A. and Paipetis, A., "Impact and after-impact properties of carbon fibre reinforced composites enhanced with multi-wall carbon nanotubes." Composites Science and Technology, 2010, 70(4), 553-563.

[25] Ashrafi, B, Guan, J, Mirjalili, V, Zhang, Y, Chun, L, Hubert, P. and et al., "Enhancement of mechanical performance of epoxy/carbon fiber laminate composites using single-walled carbon nanotubes." Composites science and technology, 2011, 71(13), 1569-1578.

[26] Soliman, E.M., Sheyka, M.P. and Taha, M.R., "Low-velocity impact of thin woven carbon fabric composites incorporating multi-walled carbon nanotubes." International Journal of Impact Engineering, 2012, 47, 39-47.

[27] Taraghi, I, Fereidoon, A. and Taheri-Behrooz, F., "Low-velocity impact response of woven Kevlar/epoxy laminated composites reinforced with multi-walled carbon nanotubes at ambient and low temperatures." Materials & Design, 2014, 53, 152-158.

[28] Tehrani, M, Boroujeni, A, Hartman, T, Haugh, T, Case, S. and Al-Haik, M., "Mechanical characterization and impact damage assessment of a woven carbon fiber reinforced carbon nanotube–epoxy composite." Composites Science and Technology, 2013, 75, 42-48.

[29] Singh, K. and Rawat, P., "Mechanical behavior of glass/epoxy composite laminate with varying amount of MWCNTs under different loadings." Materials Research Express, 2018, 5(5), 055012.

[30] Meybodi, M.H., Saber-Samandari, S, Sadighi, M. and Bagheri, M.R., "Low-velocity impact response of a nanocomposite beam using an analytical model." Latin American Journal of Solids and Structures, 2015, 12(2), 333-354.

[31] Saber Samandari, S., "Finite element modeling of polymer matrix nano-composites reinforced by nano-cylindrical fillers." International

Journal of Nano Dimension, 2014, 5(4), 371-377.

[32] Shokrieh, M. and Fakhar, M., "Experimental, analytical, and numerical studies of composite sandwich panels under low-velocity impact loadings." Mechanics of Composite Materials, 2012, 47(6), 643-658.

[33] Patil, N. and Prasad, K., "Characterization of short E-glass fiber reinforcedgraphite and bronze filled epoxy matrix composites." Iranian Journal of Materials Science and Engineering, 2016, 13(1), 28-36.

[34] Ghasemnejad, H, Soroush, V, Mason, P. and Weager, B., "To improve impact damage response of single and multi-delaminated FRP composites using natural Flax yarn." Materials & Design, 2012, 36, 865-873.

[35] Heimbs, S, Cichosz, J, Klaus, M, Kilchert, S. and Johnson A., "Sandwich structures with textile-reinforced composite foldcores under impact loads." Composite structures, 2010, 92(6), 1485-1497.

[36] Hufenbach, W, Ibraim, F. M., Langkamp, A, Böhm, R. and Hornig, A. "Charpy impact tests on composite structures–an experimental and numerical investigation." Composites Science and Technology, 2008, 68(12), 2391-2400.

[37] Sevkat, E, Liaw, B, Delale, F. and Raju, B.B., "A combined experimental and numerical approach to study ballistic impact response of S2-glass fiber/toughened epoxy composite beams." Composites Science and Technology, 2009, 69(7-8), 965-982.

[38] Akbari Aghdam, H, Bagherifard, A, Motififar, M, Parvizi, J, Sheikhbahaei, E, Esmaeili, S. and et al., "Developing A Novel Porous Bio-Photopolymer-SWCNT-Ceramic Fabricated by Digital Light Processing Technology for Orthopedic Applications." The Archives of Bone and Joint Surgery, 2020, 1-8.

[39] Chang, F-K. and Chang, K-Y., "A progressive damage model for laminated composites containing stress concentrations." Journal of composite materials, 1987, 21(9), 834-855.

[40] Chang, F-K. and Chang, K-Y., "Post-failure analysis of bolted composite joints in tension or shear-out mode failure." Journal of Composite Materials., 1987, 21(9), 809-833.

[41] Warrier, A, Godara, A, Rochez, O, Mezzo, L, Luizi, F, Gorbatikh, L. and et al., "The effect of adding carbon nanotubes to glass/epoxy composites in the fibre sizing and/or the matrix." Composites Part A: Applied Science and Manufacturing, 2010, 41(4), 532-538.